

# Optimal tuning of the control parameters of an inverter-based microgrid using the methodology of design of experiments

ISSN 1755-4535  
 Received on 24th February 2020  
 Revised 17th July 2020  
 Accepted on 10th August 2020  
 E-First on 30th September 2020  
 doi: 10.1049/iet-pel.2020.0225  
 www.ietdl.org

Jaume Miret<sup>1</sup> ✉, Pedro Paulo Balestrassi<sup>2</sup>, Antonio Camacho<sup>3</sup>, Ramón Guzmán<sup>3</sup>, Miguel Castilla<sup>1</sup>

<sup>1</sup>Electronic Engineering Department, Technical University of Catalonia, Vilanova i la Geltrú, Spain

<sup>2</sup>Institute of Industrial Engineering, Federal University of Itajuba, Itajuba, Brazil

<sup>3</sup>Automatic Control Department, Technical University of Catalonia, Vilanova i la Geltrú, Spain

✉ E-mail: jaume.miret@upc.edu

**Abstract:** The design of the control system in an inverter-based microgrid ( $\mu$ Gs) is a challenging problem due to the large number of parameters involved. Different optimisation methods based on obtaining an approximated mathematical model of the  $\mu$ G can be found in the literature. In these approaches, the non-linearities and uncertainties of the real system are typically not considered, which may result in a non-optimal tuning of the control parameters. In addition, in most applications, the problem has been simplified, assuming that all controllers have the same value for their control parameters. However, in this case, the behaviour of the system is sub-optimal since the particularities of each node of the  $\mu$ G are not taken into account. In this study, an experimental approach for tuning the control parameters of an inverter-based  $\mu$ G is introduced. The approach is based on the methodology of design of experiments and it considers different values for the control parameters of all controllers. In this study, this methodology is applied to the design of a droop-free control scheme; however, it can be easily extended to other control schemes. The validity of the proposal is verified through selected experimental results.

## 1 Introduction

In the deregulated electric market, microgrids ( $\mu$ Gs) have emerged as a promising decentralised power system that permits the integration of small-distributed generators (DGs) and provides reliability to the overall system [1, 2]. Although the  $\mu$ G can be connected to the main grid, the most challenging scenario is when it is disconnected from the mains. Then, power quality control and energy management must be performed inside the  $\mu$ G using local DG measures and some transmitted data [3, 4]. The conventional control method is based on the well-known hierarchical droop-based control [5–7]. The drawbacks of this method have been overcome by the droop-free distributed control presented in [8]. In this scheme, the primary and secondary layers of the hierarchical control are reorganised into a single control layer, which ensures the fulfilment of several objectives: fixed-frequency operation, fine voltage regulation, and accurate active and reactive power-sharing. Therefore, the interesting control in [8] is used as a base foundation for the work presented in this paper.

In recent years, the tuning of the  $\mu$ G control parameters has become a hot topic. In [9–12], small-signal  $\mu$ G models were derived to tune the parameters of the primary control layer using root-locus analysis. However, this approach does not guarantee the optimisation of the overall system response. When dealing with  $\mu$ Gs with a high number of generation nodes and complex network connections, different works deal with simplified and reduced-order mathematical models that facilitate root-locus analysis and hence parameter tuning [13–17]. Similarly, particle swarm optimisation and genetic algorithms were used in [18–23] to tune the inner voltage and current control loops as well as the active and reactive power sharing control parameters.

All these analyses apply optimisation tools to linearised system models and demonstrate that the dynamic properties are highly dependent on the loading conditions, the on/off state of the DGs, and the network parameters. In addition, most of them only demonstrate their advantages over simulated systems [10–14, 17–21]. Thus, in a real application, the inherent uncertainties such as the parasitic elements in line impedances, abrupt load connections and disconnections, non-linearity of converters and transformers, etc. can make the analytical models only a poor approximation of

the real scenario. In addition, the set of merit responses and control parameters that need to be enhanced through optimisation functions are also very limited in number due to the increasing complexity when the number of generation nodes is high [17, 19]. Another common drawback in the studies is related to the use of the same value of the control parameters in all the DGs [9, 15–20], thus obviating that the physical dispersion of the nodes will produce different behaviours between them, thereby reducing the degrees of freedom in the optimisation.

In this way, the well-established methodology of the design of experiments (DOEs), introduced by Fisher [24] and developed by Taguchi [25] and others, can be considered one of the most important methodologies for researchers who deal with experiments in practical complex applications [26]. The methodology involves running a set of experiments in the  $\mu$ G in order to obtain the most accurate information for a specific problem with the minimum number of experiments. The idea is to modify the level of all the control parameters for each experiment according to a specific experimental design. It allows a drastic reduction in the number of required experiments, provides the possibility of taking into account more control parameters and merit responses, enables the detection of interactions between parameters, and, most importantly, provides an optimised solution for the responses.

In the crowded field of inverter-based  $\mu$ G research, just a few works have used DOE in a limited way through the analysis of the tertiary hierarchical layer (energy management and scheduling) [27, 28]. Related to the primary and secondary control layers, the works that consider DOE for an optimal parameter tuning are, as far as the authors know, non-existent.

The contribution of this paper is the use of a methodology based on the design of experiments to adjust the control parameters of an inverter-based  $\mu$ G. A design procedure consisting of seven steps is proposed, which includes two random choices of control parameters: the first one to perform the initial set of experimental tests and the second one to refine the results with an additional set of tests. The novelty of the proposal is the optimisation of the control parameters using experimental results during the design process. The proposed procedure is used to design a  $\mu$ G equipped with six inverters. In this case, a total of 26 control parameters are

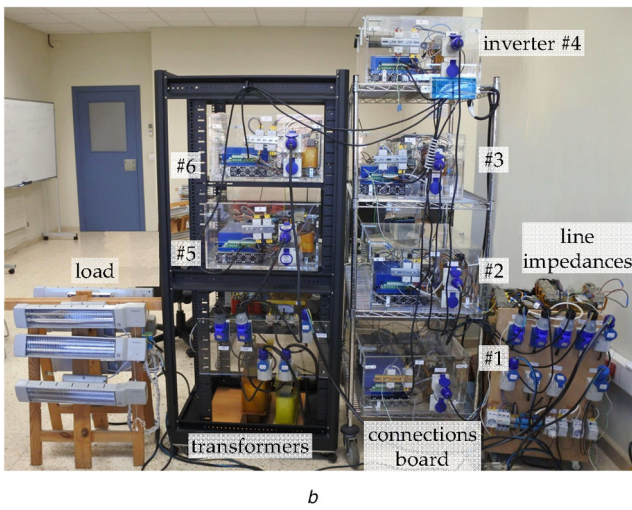
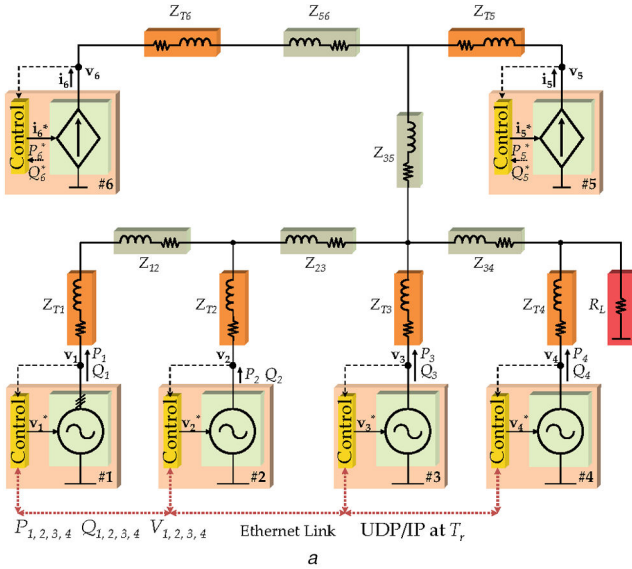


**Fig. 1**  $\mu\text{G}$  under study  
(a) Single-line diagram, (b) Photo of the three-phase laboratory setup

**Table 1**  $\mu\text{G}$  electric parameters

Symbol	Quantity	Nominal value
$V_o$	voltage (phase-to-neutral)	110 Vrms
$f_o$	frequency	60 Hz
$Z_{T_i}$	impedance of transf. $i = 1, 2$	$0.50 + j0.37 \Omega$
$Z_{T_i}$	impedance of transf. $i = 3, 4, 5$	$1.13 + j0.22 \Omega$
$Z_{T_6}$	impedance of transformer 6	$1.95 + j0.68 \Omega$
$Z_i$	line impedances $i = 12, 35$	$j0.75 \Omega$
$Z_i$	line impedances $i = 23, 34, 56$	$j0.30 \Omega$
$P_{RL}$	active power of the load	1.5–6 kW

optimised simultaneously, providing specific values for the control parameters of each inverter. The performance of this  $\mu\text{G}$  is evaluated by measuring a series of merit responses grouped into static and dynamic characteristics. The paper includes a comparison with the merit responses obtained with other control designs, showing the superiority of the proposed methodology.

## 2 System description

### 2.1 Inverter-based $\mu\text{G}$

The three-phase  $\mu\text{G}$  under study is composed of six generation nodes, which feed a load  $R_L$ , as shown in Fig. 1. The main component of each generation node is a three-phase IGBT full-bridge inverter controlled by a digital signal processor (DSP). Each

inverter is composed of a 2.3 kVA Guasch MTL-CB10060F12IXHF full-bridge converter with an LCL filter for harmonic reduction. An AMREL SPS800-12-D013 DC source emulates the primary power source of each DG.

Each node has its own DSP controller, a dual-core Texas Instruments F28M36 floating-point DSP. The control is programmed in the DSP control core, which drives the bridge switches. In order to emulate as much as possible a real  $\mu\text{G}$ , the system under study is composed of dispatchable and non-dispatchable DG nodes. Four DGs, #1 to #4, act as grid-forming nodes, i.e. operate as dispatchable power-controlled voltage sources [6, 8]. Two DG sources, #5 and #6, operate as grid-feeding nodes, which emulate intermittent renewable sources working as power-controlled current sources [29].

In the DSPs, the communication core is responsible for implementing the UDP/IP data exchange protocol at a rate of  $T_r$  seconds. Each generation node is coupled to the  $\mu\text{G}$  through an isolation transformer, represented by its equivalent impedances  $Z_{T_1}$  to  $Z_{T_6}$ . The distribution lines are emulated using impedances  $Z_{12}$ ,  $Z_{23}$ ,  $Z_{34}$ ,  $Z_{35}$ , and  $Z_{56}$ . The control of the system relies on an Ethernet communication link that provides the set points for the local controllers of each node. Table 1 lists the main electric parameters of the system.

### 2.2 Control of grid-feeding inverters

A conventional current loop drives the bridge switches of the grid-feeding inverters. In the stationary reference frame (SRF), the reference currents of this loop are written as [29]

$$i_{\alpha j}^* = \frac{2}{3} \frac{v_{\alpha j}}{v_{\alpha j}^2 + v_{\beta j}^2} P_j^* + \frac{2}{3} \frac{v_{\beta j}}{v_{\alpha j}^2 + v_{\beta j}^2} Q_j^* \quad (1)$$

$$i_{\beta j}^* = \frac{2}{3} \frac{v_{\beta j}}{v_{\alpha j}^2 + v_{\beta j}^2} P_j^* - \frac{2}{3} \frac{v_{\alpha j}}{v_{\alpha j}^2 + v_{\beta j}^2} Q_j^* \quad (2)$$

where  $v_{\alpha j}$  and  $v_{\beta j}$  are the SRF components of the output voltage, and  $P_j^*$  and  $Q_j^*$  are the power set points. It is worth mentioning that there are no control parameters to design in this power control loop.

### 2.3 Control of grid-forming inverters

A conventional cascade controller, consisting of an inner current loop and an outer voltage loop, drives the switches of the grid-forming inverters. In the SRF, the reference voltages of the outer loop are calculated as [29–31]

$$v_{\alpha j}^* = V_j^* \sin(\omega_o t + \phi_j^*) + \omega_o L_{v_j} i_{\beta j}^* \quad (3)$$

$$v_{\beta j}^* = -V_j^* \cos(\omega_o t + \phi_j^*) - \omega_o L_{v_j} i_{\alpha j}^* \quad (4)$$

where  $V_j^*$  and  $\phi_j^*$  are the references that the inverter must follow and  $L_{v_j}$  is the virtual inductance [32]. The purpose of this virtual inductance is to ensure that the total equivalent impedance formed by the series connection of the impedance seen by the converter and the virtual impedance is dominantly inductive [33, 34].

In this study, the droop-free control is used to obtain the above references, as discussed in Section 1. The reference phase is responsible to provide active power-sharing and it is computed as [8]

$$\phi_j^* = k_{iP_j} \int (\bar{P}_i - P_j) dt, \quad (5)$$

where  $P_j$  is the local active power calculated using a first-order low-pass filter of the instantaneous power  $p_j$  with a cut-off frequency  $\omega_c$ , and  $\bar{P}_i$  is the mean value of  $P_i$ , the active powers supplied by the  $m$  nodes communicated at a rate  $T_r$

$$\bar{P}_i = \frac{1}{m} \sum_{i=1}^m P_i. \quad (6)$$

The reference amplitude is responsible to realise reactive power sharing and voltage regulation. To this end, the droop-free control is implemented as [8]

$$V_j^* = V_o + V_{Q_j} + V_{V_j}, \quad (7)$$

where

$$V_{Q_j} = k_{pQ_j}(\bar{Q}_i - Q_j) + k_{iQ_j} \int (\bar{Q}_i - Q_j) dt, \quad (8)$$

$$V_{V_j} = k_{pV_j}(V_o - \bar{V}_i) + k_{iV_j} \int (V_o - \bar{V}_i) dt. \quad (9)$$

In (7)–(9),  $V_o$  is the nominal voltage amplitude, the local reactive power  $Q_j$  is calculated using a first-order low-pass filter at  $\omega_c$  and  $\bar{Q}_i$  and  $\bar{V}_i$  are the mean values of  $Q_i$  and  $V_i$ :

$$\bar{Q}_i = \frac{1}{m} \sum_{i=1}^m Q_i, \quad (10)$$

$$\bar{V}_i = \frac{1}{m} \sum_{i=1}^m V_i. \quad (11)$$

### 3 DOE for tuning the control parameters

Experimental testing is necessary before putting a complex control system into operation. In general, experimental tests are carried out once the control has been theoretically designed. In this work, these tests are incorporated into the control design process, as presented below. Note that this approach uses an offline methodology to adjust the control parameters, which are later programmed into the controller for normal operation.

The  $\mu G$  described in the previous section has 26 control parameters. The droop-free control for each grid-forming inverter has six control parameters. One parameter ( $k_{ip_j}$ ) for the active power controller in (5); two parameters ( $k_{pQ_j}$  and  $k_{iQ_j}$ ) for the reactive power controller in (8); two parameters ( $k_{pV_j}$  and  $k_{iV_j}$ ) for the voltage controller in (9) and, finally, the virtual output inductance  $L_{v_j}$ , in (3) and (4). Two other parameters are common to all the grid-forming inverters, namely the transmission rate  $T_r$  and the cut-off frequency of the active and reactive power filters  $\omega_c$ . As mentioned above, the grid-feeding inverters have no control parameters in (1) and (2). Therefore, these inverters are not considered in the control design of the  $\mu G$ .

The simplest approach for the design would be to choose the controller parameters equally in all the nodes; however, in this case, there is no evidence to show that all the merit responses that describe the dynamic behaviour are optimised.

In order to provide a more effective approach, DOE techniques will be used to retrieve the optimal control parameters [26]. The principle of DOE is to realise a set of experiments in order to obtain the most accurate information for a specific problem with the minimum number of experiments [35]. The idea is to modify the level of multiple parameters for each experiment according to a specific design. It allows a drastic reduction in the number of required experiments, provides the possibility of taking into account more parameters, enables the detection of interactions between parameters using statistical tools, and provides an optimised solution for the considered responses. The common guidelines cover seven steps, as shown in Fig. 2.

#### 3.1 Statement of the problem

The first step is to establish a clear statement of the problem; in this case, it is to optimise the behaviour of the  $\mu G$  depicted in Fig. 1. Therefore, the  $\mu G$  must be tested following a predefined sequence

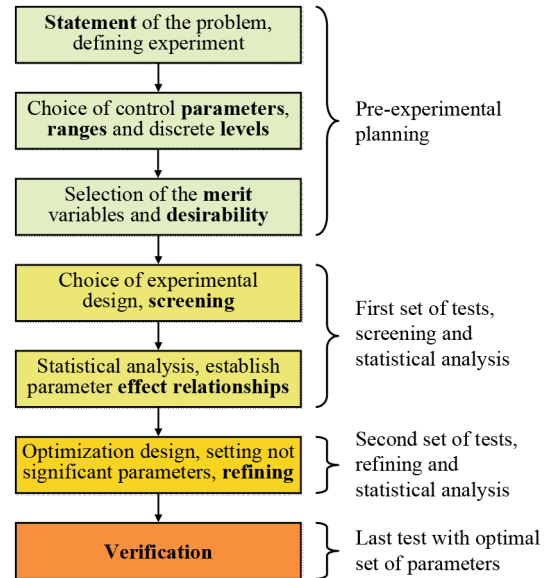


Fig. 2 Algorithm for designing an experiment

of events that permit the evaluation of its dynamics and its steady-state performance by collecting the most relevant data. A test with different events will be programmed in the  $\mu G$ : a start-up with the grid-forming inverter #1 feeding the load at low power (1.5 kW), and a sequential start-up of the other grid-forming inverters. The last event will be the start-up of inverter #4, which is programmed to ensure that the  $\mu G$  is in the steady state. At this time, different merit responses (transitory and steady state) are defined to evaluate the system behaviour. Note that the grid-feeding inverters will be inactive in this initial test.

#### 3.2 Choice of parameters, ranges and levels

As mentioned above, the laboratory  $\mu G$  presents 26 control parameters to be tuned appropriately. Multiple experiments will be carried out by varying the parameters following a predefined scheme. Three sets of experiments will be performed consecutively: the screening set, the refining set, and a final test to verify that an optimal solution has been obtained; as shown in Fig. 2.

In the first step (screening), each experiment will be performed with a randomised set of control parameters with only two discrete value levels per parameter. This randomised choice starts the search for the optimum space of solutions. The discrete levels of the parameters are selected by considering the following: first, the maximum and minimum ranges of the parameters defined by the designers and, second, two discrete values for each parameter. These two discrete values are calculated by considering the Tchebichev rule for standard deviation, which roughly states that at least 3/4 of the data lie within two standard deviations of the mean. Table 2 lists the values for each parameter for screening. It must be noted that the minimum and maximum values of the control parameters are chosen by the designers based on their practical expertise, as commonly done in the state-of-the-art optimisation methods [18–23].

#### 3.3 Choice of merit responses, weights, and importance

Since the main objective of the controller is to share the active and reactive powers equally between the converters, the maximum deviations of the measured active and reactive powers generated by each node from their ideal values ( $e_{P_s}$ ,  $e_{Q_s}$ ) will, respectively, be the first and second merit responses to be assessed. This concept is also used in the other merit responses shown in Table 3.

The third chosen response will be the  $\mu G$  mean voltage deviation from the nominal value  $e_{V_s}$ . The fourth merit response will be the voltage ripple in each node  $R_V$ . These responses are only related to steady-state objectives, and therefore some dynamic merit responses should be defined. As stated before, since the

**Table 2** Control parameters levels for screening

Parameter	Minimum	Maximum	Mean	Std. Dev.	Level 1	Level 2	Units
$k_{iPj}$	0.1	1.0	0.55	0.225	0.325	0.775	(kW $s^2$ ) $^{-1}$
$k_{pQj}$	0.1	1.0	0.55	0.225	0.325	0.775	mA $^{-1}$
$k_{iQj}$	1	10	5.50	2.250	3.250	7.775	m(As) $^{-1}$
$k_{pVj}$	0	50	25.25	12.375	12.875	37.625	m
$k_{iVj}$	50	500	275	112.5	162.5	387.5	ms $^{-1}$
$L_{vj}$	1	10	5.5	2.25	3.25	7.75	mH
$T_r$	50	1000	525	237.5	287.5	762.5	ms
$\omega_c$	$2\pi$	$12\pi$	$7\pi$	$2.5\pi$	$4.5\pi$	$9.5\pi$	rad/s

**Table 3** Merit responses with lower and upper limits, weights and importance

Merit response	Definition	Lower	Upper	Weight	Importance	Units
$e_{Ps}$	$\max  (P_j - \bar{P}_j)/\bar{P}_j $	0	10	10	10	%
$e_{Qs}$	$\max  (Q_j - \bar{Q}_j)/\bar{Q}_j $	0	10	10	5	%
$e_{Vs}$	$ (V_o - \bar{V}_j)/\bar{V}_j $	0	10	1	5	%
$R_V$	$\max$ (ripple ( $P_j - P_{jss}$ ))	0	0.05	10	1	p.u.
$\Delta P$	$\max  (P_j - P_{jss}) $	0	500	1	1	W
$\Delta Q$	$\max  (Q_j - Q_{jss}) $	0	500	1	1	VA
$\Delta V$	$\max  (V_j - V_{jss}) $	0	0.1	1	1	p.u.
$t_{sP}$	$\max (t_{sPj})$	0	10	1	1	s
$t_{sQ}$	$\max (t_{sQj})$	0	10	1	1	s
$t_{sV}$	$\max (t_{sVj})$	0	10	1	1	s

system is in steady state, node #4 starts up, which produces different overshoots and settling times in the powers and voltages. Six additional merit responses can be established by measuring the overshoot ( $\Delta P$ ,  $\Delta Q$ , and  $\Delta V$ ) and settling time ( $t_{sP}$ ,  $t_{sQ}$ , and  $t_{sV}$ ) to reach a steady state. The step-change settling time is defined as the time required for the response curves (i.e. active power transient response against a step load change) to reach and stay within a range of 5% of its steady-state value. The merit response is chosen as the maximum (worst) settling time among the four converters.

Table 3 also includes two additional columns, which will be necessary to run the so-called desirability method (better described in Section 3.5). This method will be used to optimise the multiple responses simultaneously. These additional columns are for the desired lower and upper limits for the merit responses, the individual desirability weights, and the relative importance of the responses. The lower limit will be the target value of 0 in the optimisation problem. The upper limit will be the desirable maximum of the merit responses. The next column is the weight; it determines how the desirability function is distributed on the interval between the upper bound and the target for an optimisation problem. It determines the shape of the desirability function that is used to translate the response scale to the zero-to-one desirability scale in order to determine the individual desirability of a response. One can select a weight from 0.1 to 10 to emphasise or de-emphasise the necessity of hitting the target value: a weight equal to 1 places equal importance on the target and the bounds. This is a neutral setting. A weight is higher than 1 places more emphasis on the target. Increasing the weight requires the response to move closer to the target to achieve a specified desirability. In this case, the deviations of  $P$  and  $Q$  ( $e_{Ps}$  and  $e_{Qs}$ ) and the voltage ripple ( $R_V$ ) present the higher weights. The last factor is the importance of the merit responses. It determines the amount of effect each response has on the composite desirability. If all the responses are equally important, the default value is 1 for each response. However, in this study, the  $P$  overshoot has a higher importance value, because it can disconnect the inverter if the protection limits are reached. Thus, the optimisation of these merit responses (outputs,  $Y$ ) by choosing the optimal set of control parameters (inputs,  $X$ ) represents a complex multiple and multivariate  $Y = f(X)$  problem where several responses need to be jointly optimised.

To summarise, the objective is to optimise ten merit responses, each one with a relevance weighed by the experience of the designer. Obviously, changing the subjective relevance responses (i.e. weight and importance columns in Table 3) will bring a different set of optimised control parameters in all the optimisation methods with more than one merit response [18–23]. When dealing with a  $\mu G$  with specific characteristics, the researchers can weigh the objectives differently but the procedure will be the same.

The participation of expert designers is necessary during the pre-experimental planning, as shown in Fig. 2. The definition of the limits for the control parameters and merit responses as well as the weight and importance factors in Tables 2 and 3 is based on their practical expertise. However, the rest of the design procedure leading to the optimal control solution can be applied without the need for previous experience in control design.

### 3.4 Choice of experimental design and screening

The term design denotes a matrix where the columns represent the input parameters and each row represents a combination of the chosen parameter levels (presented in Table 2). Therefore, a randomised combinatorial set of the chosen discrete levels must be determined with the aim of taking the most accurate view of the complete combinatorial possibilities (which are, of course, impossible to test in laboratory experiments). In the screening phase, the goals are to identify those parameters that may affect the performance the most, screen out the irrelevant parameters, and establish the tentative cause and effect relationships. In this work, the statistical software package Minitab has been used to choose an appropriate 2-level design based on the number of control parameters that are of interest, the number of runs one can perform, and the desired resolution of the design. In this case, the so-called Plackett–Burman design is the first choice for this screening phase. Plackett–Burman designs are usually resolution III, 2-level designs [25]. In a resolution III design, the main effects are aliased with 2-factor interactions. Therefore, these designs should only be used when it can be assumed that 2-factor interactions are negligible. Plackett–Burman designs are used to identify the most important factors early in the experimentation phase. Minitab generates the designs for up to 47 factors. Each design is based on the number of runs, from 12 to 48, and is always a multiple of 4. The number of

**Table 4** Resolution 3 Plackett–Burman screening

Test	$T_r$	$k_{iP1}$	$k_{iP2}$	$k_{iP3}$	$k_{iP4}$	$\omega_c$
1	762.5	0.325	0.775	0.775	0.775	14.135
2	762.5	0.775	0.325	0.775	0.775	29.845
3	762.6	0.775	0.775	0.325	0.325	29.845
25	287.5	0.775	0.325	0.775	0.325	29.845
26	287.5	0.325	0.775	0.325	0.775	14.135
27	287.5	0.775	0.325	0.325	0.325	29.845
28	287.5	0.325	0.325	0.325	0.325	14.135

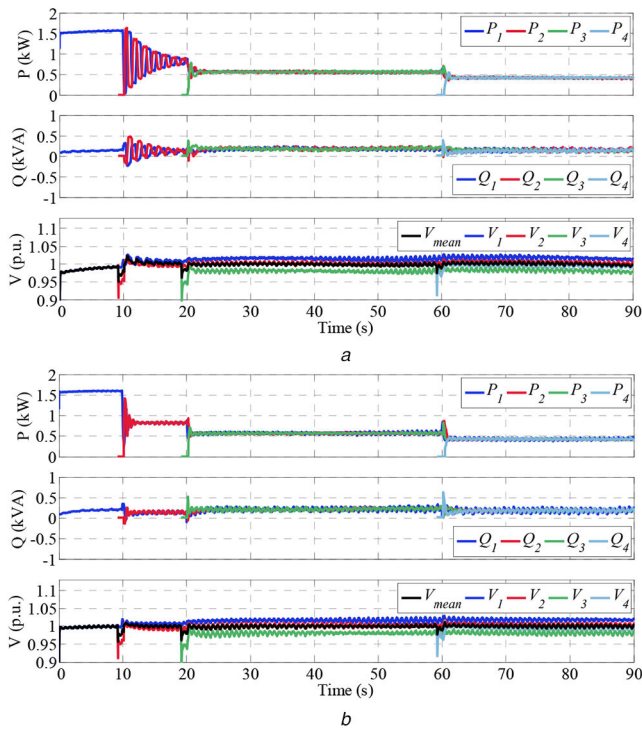


**Fig. 3** Experimental tests under different sets of non-optimised control parameter values in the screening phase  
(a) Test 3, (b) Test 25

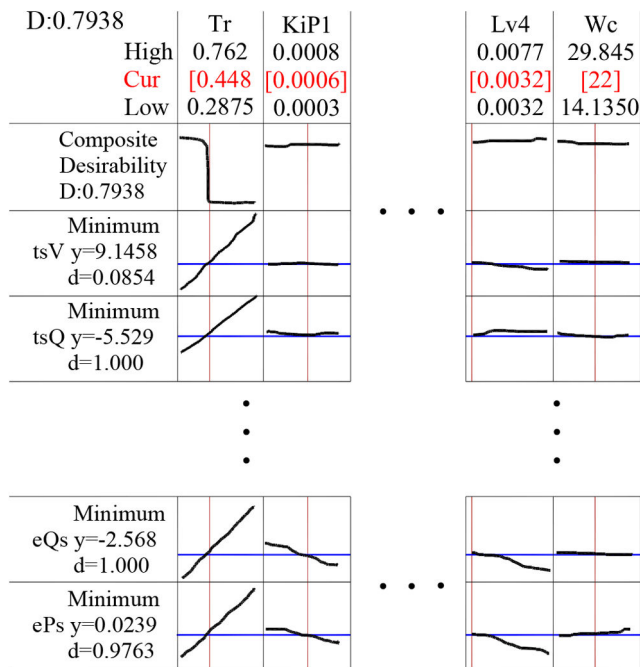


**Fig. 4** Optimisation plot showing how the parameters affect the predicted responses

factors must be less than the number of runs. For example, a design with 28 runs (our case) lets us estimate the main effects for up to 26 factors. Table 4 shows the factorial experimental designs for some of the 26 parameters to be tuned.

For each row, corresponding to an experimental run, 10 merit responses must be measured after the experimental test.

Fig. 3 shows the experimental results for two different runs (test 3 and test 25). At  $t=0$  s, node #1 starts to energise the  $\mu$ G supplying the common load  $R_L$  on its own. At  $t=10$  s, node #2 is started and load sharing begins. Node #3 is started at  $t=20$  s, and for 40 s, the three inverters share the load. At  $t=60$  s, node #4 is started. This long time-gap between starting #3 and #4 is useful to ensure a perfectly stabilised steady state before #4 is started. Thus, all the merit response definitions and measurements will be done from  $t=60$  s to  $t=90$  s. The top subfigure shows the active power  $P_j$  supplied by each node. The middle subfigure shows the reactive power  $Q_j$  of the individual nodes. The bottom subfigure shows the per unit (p.u.) output voltage of each node  $V_j$  and also the mean value of the output voltage of the four nodes  $V_{mean}$ . As it can be seen, in the steady state, the three objectives of the droop-free control are fulfilled: active and reactive power sharing between nodes, and setting the mean voltage value (black line) to 1 p.u. In addition, these tests are done with a non-optimised set of parameters. For example, a large voltage settling time is appreciated when running test 3 compared with that when running test 25. In addition, when starting converter #2, both tests present active power oscillations that must be avoided.

### 3.5 Statistical analysis

After running the 28 tests described in the last subsection, the considered merit responses were measured for each test, and the entire data was analysed. From this screening analysis, some results were established, considering all the merit responses and control parameters. Stepwise regression (mainly using the forward selection method) was used to select the independent models for all the merit responses. Stepwise regression is an automated tool used in the exploratory stages of model building to identify a useful subset of predictors. The process systematically adds the most significant parameter or removes the least significant parameter during each step. The forward selection procedure to estimate the terms of a model starts with an empty model and adds the most significant term for each step. The procedure stops when all the parameters that are not in the model have  $p$ -values greater than the specified alpha-to-enter value. See (12), for example which shows the dependence of the merit response  $e_{Ps}$  on the significant parameters and interactions. Similar equations were obtained for all the ten merit responses.

$$\begin{aligned}
 e_{Ps} = & -5.504 + 23.03T_r + 2017k_{pQ2} - 616k_{pQ3} \\
 & -3762k_{pQ4} + 3.353k_{iV3} + 670.4L_{v1} + 457.7L_{v4} \\
 & -6492T_r k_{pQ2} + 10193T_r k_{pQ4} - 2158T_r L_{v1} - 903T_r L_{v4}
 \end{aligned} \tag{12}$$

After obtaining the ten merit response models, the desirability function is used as the optimisation procedure. The optimisation plot in Fig. 4 shows how the parameters affect the predicted responses. Each column of the graph corresponds to one of the 26 parameters. The top row of the graph corresponds to the composite desirability,  $D$ . Each remaining row corresponds to one of the ten

**Table 5** Parameter settings and levels for refining

Parameter	Set	Level 1	Level 2	Parameter	Set	Level 1	Level 2
$k_{iP1}$	0.550	—	—	$k_{pV1}$	22.250	—	—
$k_{iP2}$	0.325	—	—	$k_{pV2}$	12.875	—	—
$k_{iP3}$	0.325	—	—	$k_{pV3}$	12.875	—	—
$k_{iP4}$	0.775	—	—	$k_{pV4}$	37.625	—	—
$k_{pQ1}$	0.325	—	—	$k_{iV1}$	275	—	—
$k_{pQ2}$	—	0.1	0.574	$k_{iV2}$	387.5	—	—
$k_{pQ3}$	—	0.1	0.556	$k_{iV3}$	—	239.3	500
$k_{pQ4}$	—	0.1	0.590	$k_{iV4}$	—	230	500
$k_{iQ1}$	3.25	—	—	$L_{v1}$	—	7.3	10
$k_{iQ2}$	3.25	—	—	$L_{v2}$	7.750	—	—
$k_{iQ3}$	3.25	—	—	$L_{v3}$	3.250	—	—
$k_{iQ4}$	7.75	—	—	$L_{v4}$	—	6.3	10
$T_r$	—	50	488	$\omega_c$	22	—	—

merit responses. The numbers displayed at the top of a column show the current parameter settings (in red) and the high and low control parameter settings in the experimental design. At the left of each response row, Minitab shows the goal of the response, the predicted response  $y$  at the current parameter settings, and the individual desirability score  $d$ . The composite desirability is displayed in the top row and the upper left corner of the graph. The vertical red lines on the graph represent the current settings. The horizontal blue lines represent the current response values. The grey regions indicate where the corresponding response has zero desirability. The desirability function involves transforming each estimated merit response  $\hat{y}_i$  into an individual desirability value  $d_i$ , where  $0 \leq d_i \leq 1$ . The individual desirabilities are combined through a simple geometric mean weight ( $z_i$ ), as

$$D = (d_1^{z_1} d_2^{z_2} \dots d_k^{z_k}) \left( \sum_i^k z_i \right)^{-1} \quad (13)$$

These weights indicate the importance of each property in relation to the others in the multi-objective optimisation process, where  $k$  is the number of responses and the value  $D$  ensures the global composite desirability. The combination of the individual desirability for each level of response and its values are in the interval  $[0, 1]$ . To minimise the merit response ( $y$ ) obtained by stepwise regression through the desirability function, a transformation of variables was used according to

$$D[y] = \begin{cases} 0 & \text{if } \hat{y}_i > H_i \\ \left( \frac{L_i - \hat{y}_i}{H_i - T_i} \right)^\lambda & \text{if } T_i \leq \hat{y}_i \leq H_i \\ 1 & \text{if } \hat{y}_i < T_i \end{cases} \quad (14)$$

where  $L_i$  is the lower limit of desirability,  $H_i$  is the upper limit of desirability,  $T_i$  is the target of the desirability, and  $\lambda$  is a parameter of desirability. When  $\lambda \sim 1$ , equal emphasis is given to the target and limits; when  $\lambda \sim 10$ ,  $\hat{y}_i$  assumes a value closer to the target [36, 37].

As an example, from Fig. 4, it can be seen that low values of parameter  $T_r$  provides a high  $D$ , and with an abrupt step change, high values of  $T_r$  worsens  $D$ . Also, it is shown in Fig. 4 that low values of  $T_r$  produce low steady-state errors in  $P$  and  $Q$  sharing, and high values of  $T_r$  worsens  $P$  and  $Q$  sharing.

From this screening analysis, some results were established, considering all the 10 merit responses and 26 control parameters, as shown in Table 5.

(i) Some control parameters were considered not significant when changing the parameter levels in all the responses. Further designs could consider them as noise parameters. These parameter levels

were established according to the best desirability value. These values will be fixed in subsequent experimental designs.

(ii) The parameter  $\omega_c$  was considered significant for all the designs at 22 rad/s.

(iii) The parameters  $T_r$ ,  $k_{pQ2}$ ,  $k_{pQ3}$ ,  $k_{pQ4}$ ,  $k_{iV3}$ ,  $k_{iV4}$ ,  $L_{v1}$ , and  $L_{v4}$  were considered borderlines because it was not clear whether to eliminate or select the parameter level. Here, further investigation is needed.

### 3.6 Optimisation design and refining

From Table 5, it can be seen that some parameters are fixed with this first step and some need to be adjusted in the second DOE step or refining phase. For these parameters, two new randomised levels are defined for the refining phase. This second randomised choice initiates the search of the global control solution avoiding the local optimum points. Table 6 shows the factorial design experimental plan for the refining phase of the parameter tuning. In this phase, 16 experiments are required. This is a natural choice in Minitab software, considering that in a resolution IV fractional design, the main effects are not aliased with any other main effect or 2-factor interactions, but some 2-factor interactions are aliased with other 2-factor interactions and the main effects are aliased with 3-factor interactions.

After performing the refining tests and measuring their merit responses, a new statistical analysis must be done, resulting in a new optimisation plot. Taking into account this optimisation plot in Fig. 5, the results show that all the parameters are somehow influential on the merit responses. Some findings are as follows:

(i) The parameters  $k_{pQ3}$  and  $k_{pQ4}$  have more influence on the composite desirability in their upper levels.

(ii) The parameters  $k_{pQ2}$ ,  $k_{iV3}$ ,  $L_{v1}$ , and  $L_{v4}$  have more influence on the composite desirability in their lower levels.

(iii) The  $T_r$  parameter has an optimal value at 0.267 ms and can worsen the composite desirability on the extreme values.

From this last phase, the final and optimal tuning for the parameters were obtained, as shown in Table 7.

As a final remark, note that in the proposed DOE approach, the stability is checked by testing the  $\mu G$  experimentally. The worst values of the control parameters, even those that can make the system unstable, are discarded in the different design steps (screening, statistical analysis, optimisation design, etc.), which are performed by running different sets of experiments. Therefore, the final set of control parameters guarantees the best static and dynamic performance according to the defined merit factors and also system stability. The relevance of this approach is that stability is ensured in the real scenario where the  $\mu G$  has to operate, with all the practical imperfections of the real system such as parasitic elements, non-linearities, and uncertainties.

**Table 6** Resolution IV fractional factorial design

Test	$T_r$	$k_{pQ2}$	$k_{pQ3}$	$k_{pQ4}$	$k_{iV3}$	$k_{iV4}$	$L_{v1}$	$L_{v4}$
1	50	0.1	0.1	0.1	239.3	230	7.3	6.3
2	50	0.574	0.1	0.1	500	230	10	10
3	50	0.1	0.556	0.1	500	500	10	6.3
4	50	0.574	0.556	0.1	239.3	500	7.3	10
5	50	0.1	0.1	0.59	500	500	7.3	10
6	50	0.574	0.1	0.59	239.3	500	10	6.3
7	50	0.1	0.556	0.59	239.3	230	10	10
8	50	0.574	0.556	0.59	500	230	7.3	6.3
9	448	0.1	0.1	0.1	239.3	500	10	10
10	448	0.574	0.1	0.1	500	500	7.3	6.3
11	448	0.1	0.556	0.1	500	230	7.3	10
12	448	0.574	0.556	0.1	239.3	230	10	6.3
13	448	0.1	0.1	0.59	500	230	10	6.3
14	448	0.574	0.1	0.59	239.3	230	7.3	10
15	448	0.1	0.556	0.59	239.3	500	7.3	6.3
16	448	0.574	0.556	0.59	500	500	10	10

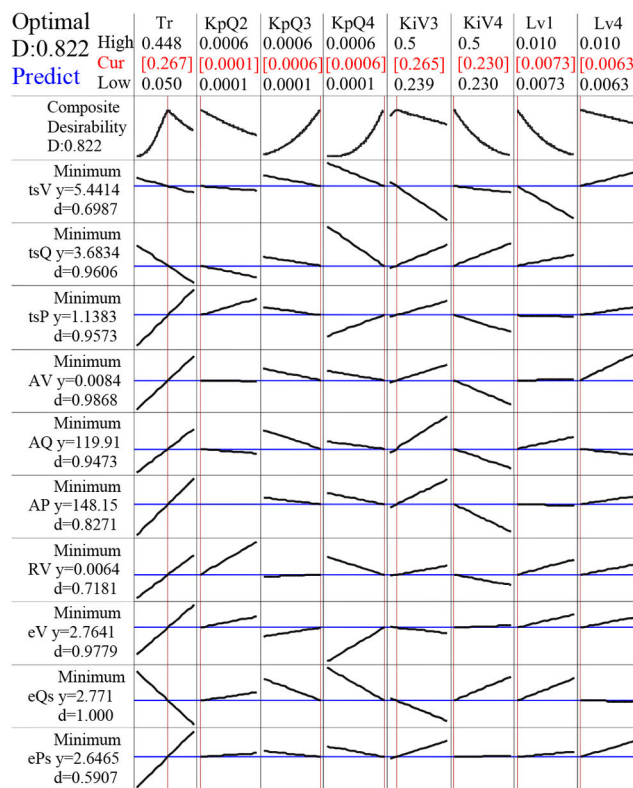


**Fig. 5** Optimisation plot in the refining phase

**4 Experimental verification**

**4.1 Validating the optimal control solution**

A final test with the set of optimal parameters must be done to confirm that an optimal response has been obtained. Fig. 6 shows the transient response of the system when using the optimised set of control parameters. The last two columns in Table 7 list the measured merit responses when running this experiment. As can be seen, the behaviour of the  $\mu G$  is now fine-tuned compared to the results shown in Fig. 3.

**4.2 Sensitivity analysis**

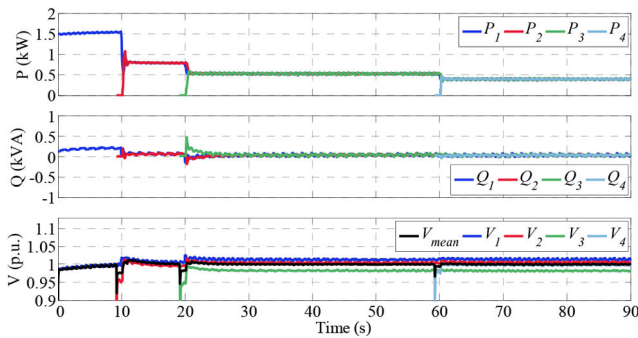
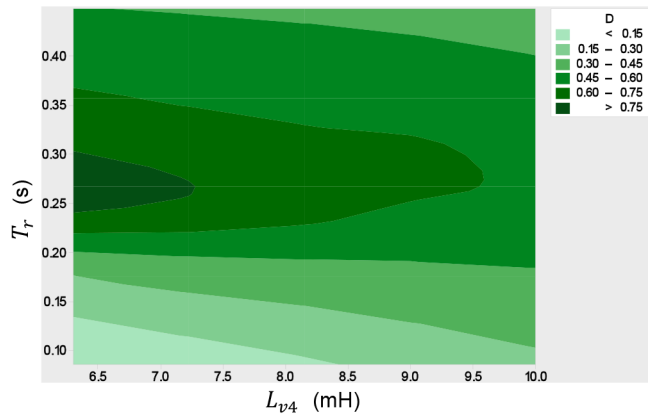
An evaluation of the variations of the composite desirability  $D$  when changing some of the optimised parameters can provide useful information to the designer. Fig. 7 shows the sensitivity analysis for the composite desirability values when  $T_r$  and  $L_{v4}$  are varying around their optimal values. As shown in Fig. 7, the

optimal value  $T_r = 0.267$  s provides the highest composite desirability. Clearly, system performance worsens when the speed at which controllers receive data becomes slower ( $T_r > 0.267$  s). However, the performance also worsens when the speed is too fast ( $T_r < 0.267$  s), probably due to the slow dynamics of the control signals. Note that these signals are processed by low-pass filters with cut-off frequencies lower than the frequency of the  $\mu G$  (see Table 7). Similarly, the optimal value of  $L_{v4}$  gives the highest desirability; as shown in Fig. 7. In this case, the impedance seen at the output of the inverter #4 is sufficiently inductive with this optimal value, which guarantees the best result in the merit responses.

Three new tests mismatching the optimised parameter set were conducted to corroborate the findings of the composite desirability plot shown in Fig. 7. The first one reduces the transmission rate to  $T_r = 0.1$  s, the second one increases  $T_r$  to 0.5 s, and the third one increases  $L_{v4}$  to 10 mH. The improvements of the merit responses

**Table 7** Optimised parameters and measured responses

Parameter	Set	Parameter	Set	Responses	Value
$k_{iP1}$	0.550	$k_{pV1}$	22.250	$e_{Ps}$	0.3%
$k_{iP2}$	0.325	$k_{pV2}$	12.875	$e_{Qs}$	2.1%
$k_{iP3}$	0.325	$k_{pV3}$	12.875	$e_{Vs}$	1.4%
$k_{iP4}$	0.775	$k_{pV4}$	37.625	$\Delta P$	70.1 W
$k_{pQ1}$	0.325	$k_{iV1}$	275	$\Delta Q$	73.8 VA
$k_{pQ2}$	0.100	$k_{iV2}$	387.5	$\Delta V$	5.2 mp.u.
$k_{pQ3}$	0.600	$k_{iV3}$	265.7	$R_V$	7 mp.u.
$k_{pQ4}$	0.600	$k_{iV4}$	230	$t_{sP}$	~1 s
$k_{iQ1}$	3.25	$L_{v1}$	7.30	$t_{sQ}$	~1 s
$k_{iQ2}$	3.25	$L_{v2}$	7.75	$t_{sV}$	~1 s
$k_{iQ3}$	3.25	$L_{v3}$	3.25	—	—
$k_{iQ4}$	7.75	$L_{v4}$	6.30	—	—
$T_r$	267	$\omega_c$	22	—	—

**Fig. 6** Experimental response using the optimised set of control parameters**Fig. 7** Desirability contour plot

of the optimised solution in front of the results of the mismatched cases are listed in Table 8. The improvements are calculated as

$$I(mr_{opt}) = 100 \frac{mr_{mism} - mr_{opt}}{mr_{mism}}, \quad (15)$$

where  $mr_{opt}$  and  $mr_{mism}$  denote the merit response using the optimised and mismatched control parameters, respectively. Note that a positive (negative) value of  $I(mr_{opt})$  means that the optimised solution improves (worsens) the merit response respect to the mismatched case. It is worth remembering that the merit factors have different weight and importance; as shown in Table 3. Therefore, the quality of the solution will be given by the highest value in  $I(e_{Ps})$  since this is the merit factor with the largest weight and importance. With this in mind, it is clear that the optimised solution offers the best results with improvements of up to  $I(e_{Ps}) = 40\%$  in the  $e_{Ps}$  merit factor.

**Table 8** Response improvement in front of mismatched parameters

$I(mr_{opt})$	$T_r$ 0.1 s	$T_r$ 0.5 s	$L_{v4}$ 10 mH
$I(e_{Ps})$	40%	0%	40%
$I(e_{Qs})$	49%	0%	34%
$I(e_{Vs})$	18%	12%	0%
$I(R_V)$	-23%	-17%	-7.7%
$I(\Delta P)$	25%	43%	4.2%
$I(\Delta Q)$	-5.9%	6.5%	-1.2%
$I(\Delta V)$	16%	15%	0%

**Table 9** Designs with identical control parameters

Design	$k_{iP}$	$k_{pQ}$	$k_{iQ}$	$k_{pV}$	$k_{iV}$	$L_v$
mean	0.494	0.406	4.375	21.406	289.5	6.15
min	0.325	0.325	3.250	12.875	230.0	3.25
max	0.775	0.600	7.750	37.625	387.5	7.75

#### 4.3 Comparison with other control design approaches

Typically, the design of  $\mu$ Gs with multiple inverters is performed, assuming that all the controllers have the same values for the control parameters [9, 15–20]. This subsection considers three variants of this approach to enrich the comparison. The criteria for selecting the parameters are to use the mean, minimum or maximum values. Table 9 lists the parameters for these designs.

Three new experimental tests were carried out to compare the merit factors of the proposed design with those obtained with the designs that use identical control parameters. In this case, the response improvement was defined as

$$I(mr_{opt}) = 100 \frac{mr_{ident} - mr_{opt}}{mr_{ident}}, \quad (16)$$

where  $mr_{ident}$  denotes the merit response using one of the designs with identical parameters. The results are shown in Table 10. As it was indicated in the previous subsection, the quality of the solution is measured by the highest value in  $I(e_{Ps})$ . In this comparison, it is clear that the improvement obtained with the optimised parameter set is very good, with  $I(e_{Ps})$  ranging from 25 to 67%. These excellent results validate the superior performance of the proposed solution.

#### 4.4 Operation with variable production and demand

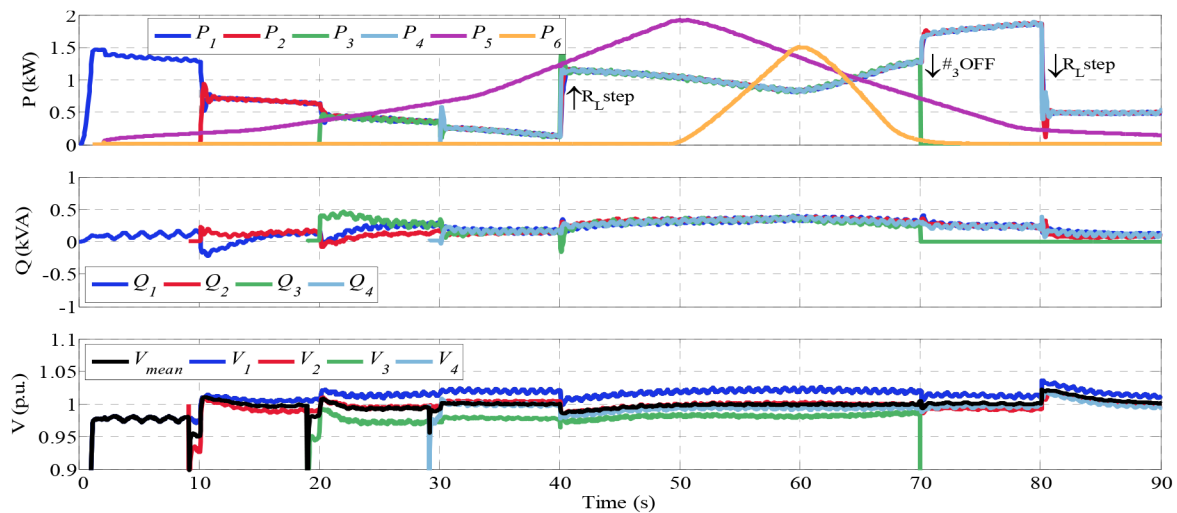
The effectiveness of the proposal was validated in a new scenario with variable production and demand. To this end, the chronogram shown in Table 11 was considered. The experiment includes the operation of the four grid-forming inverters (#1 to #4), which

**Table 10** Response improvement for designs with identical parameters

$I(mr_{opt})$	Mean	Min	Max
$I(e_{p_s})$	50%	67%	25%
$I(e_{Q_s})$	-11%	49%	-91%
$I(e_{V_s})$	6.7%	6.7%	12%
$I(R_V)$	-15%	-80%	2.8%
$I(\Delta P)$	-3.5%	-33%	15%
$I(\Delta Q)$	-59%	72%	16%
$I(\Delta V)$	1.9%	3.7%	30%

**Table 11** Chronogram for the test in Fig. 8

Time, s	Element	Event
0	Inverter #1 (grid-forming)	OFF → ON
0	load connection	0 kW → 1.5 kW
2	Inverter #5 (grid-feeding)	OFF → ON
10	Inverter #2 (grid-forming)	OFF → ON
20	Inverter #3 (grid-forming)	OFF → ON
30	Inverter #4 (grid-forming)	OFF → ON
40	load increase	1.5 kW → 6 kW
50	Inverter #6 (grid-feeding)	OFF → ON
70	Inverter #3 (grid-forming)	ON → OFF
70	Inverter #6 (grid-feeding)	ON → OFF
80	Load decrease	6 kW → 1.5 kW

**Fig. 8** Operation of the  $\mu G$  with variable production and demand

emulate dispatchable DG sources and the two grid-feeding inverters (#5 and #6) which operate as non-dispatchable DG sources.

Fig. 8 shows the experimental results. The power generation profiles of inverters #5 and #6 are shown in the top subfigure. These profiles are set by the extraction of the maximum power from two renewable energy sources. In this subfigure, it is clear that the grid-forming inverters perfectly share the active power in this variable production and demand scenario. Note that, from  $t = 0$  s to  $t = 40$  s, the active power of these inverters is being reduced as the production of the non-dispatchable sources increases. In  $t = 40$  s, a step load change from 1.5 to 6 kW is produced and, consequently, the active power of the inverters #1 to #4 experiences an abrupt and fast increase. In  $t = 70$  s, the inverter #3 is disconnected and the rest of grid-forming inverters continue to share the active power correctly. In  $t = 80$  s, there is an abrupt power reduction in inverters #1, #2, and #4 due to a load change from 6 to 1.5 kW.

Fig. 8 (middle subfigure) shows the reactive power of the grid-forming inverters. During the black start of the  $\mu G$ , some deviations in reactive power can be noticed (from  $t = 10$  s to  $t = 30$  s). However, it is clear that a good power-sharing is achieved in

steady state, as desired. In this test, the grid-feeding inverters #5 and #6 are programmed to extract the maximum power of the intermittent sources and not to inject reactive power ( $Q_5^* = 0$  and  $Q_6^* = 0$ ). Therefore, the reactive power of these inverters is not shown in Fig. 8.

Fig. 8 (bottom subfigure) shows the output voltage of the grid-forming inverters. As expected, the mean voltage of the  $\mu G$  is correctly regulated at 1 p.u. in a steady state; see the black waveform.

## 5 Conclusion

In this study, the design of experiment methodology was applied to obtain the best set of control parameters in order to optimise the behaviour of an inverter-based  $\mu G$ . The chosen approach is based on the factorial design of experiments using screening and fractional factorialisation. This work provided a procedure that finds the desirability function for a multiple and multivariate problem with 26 control parameters and 10 merit responses. This procedure finds a solution that takes into account the real behaviour of the  $\mu G$ , through testing in an experimental setup. This

approach takes into account parasitic elements, nonlinearities and uncertainties that are inherently present in the setup and that are not typically included in theoretical small-signal models. In addition, the procedure provides a specific solution for the control parameters of each node, thus allowing a particular optimisation to each generation node of the  $\mu$ G. Finally, the experimental measurements show that the main objective of optimising the dynamical system behaviour was successfully accomplished, even in scenarios with variable production and demand. In addition, the experimental study reveals that the proposal is effective for the integration of non-dispatchable DG sources in islanded  $\mu$ Gs.

An open topic for future research is the application of the design of experiment methodology to different scenarios. For instance, the procedure proposed in this work can be easily applied to  $\mu$ Gs that supply non-linear loads or to optimise the system operation under communication issues to mention two significant examples. In this last case, the experimental tests in the screening and refining steps must be redefined by programming delays in the communication channels, loss of data packets, and even loss of communication links. However, the design procedure should maintain the proposed merit factors to ensure the optimal set of control parameters. The extension of the design methodology to other control algorithms is a more challenging issue. For instance, algorithms for sharing the voltage and current harmonics in polluted microgrids can be considered. In this case, the design procedure must be modified at several points. First, the control parameters for harmonic sharing must be included in the pre-experimental planning step. Second, new merit responses related to voltage and current harmonic sharing must be selected and third, the screening and refining steps must be updated taking into consideration the number of control parameters and the number of needed tests for optimisation. In any case, the main ideas for carrying out an optimal design based on experiments have been described in this work and their application can be extended to the design of controllers for harmonic sharing or for other complex control problems.

## 6 Acknowledgments

This work was supported by the Ministry of Science, Innovation and Universities of Spain and by the European Regional Development Fund under project RTI2018-100732-B-C22.

## 7 References

[1] Peças Lopes, J.A., Moreira, C.L., Madureira, A.G.: 'Defining control strategies for microgrids islanded operation', *IEEE Trans. Power Syst.*, 2006, **21**, (2), pp. 916–924

[2] Yahaya, A.A., AlMuhaini, M., Heydt, G.T.: 'Optimal design of hybrid DG systems for microgrid reliability enhancement', *IET Gener. Transm. Distrib.*, 2020, **14**, (5), pp. 815–823

[3] Peng, Z., Wang, J., Wen, Y., *et al.*: 'Virtual synchronous generator control strategy incorporating improved governor control and coupling compensation for AC microgrid', *IET Power Electron.*, 2019, **12**, (6), pp. 1455–1461

[4] Mishra, S., Mallesham, G., Jha, A.N.: 'Design of controller and communication for frequency regulation of a smart microgrid', *IET Renew. Power Gener.*, 2012, **6**, (4), pp. 248–258

[5] Vasquez, J.C., Guerrero, J.M., Miret, J., *et al.*: 'Hierarchical control of intelligent microgrids', *IEEE Ind. Electron. Mag.*, 2010, **4**, (4), pp. 23–29

[6] Nutkani, I.U., Loh, P.C., Blaabjerg, F.: 'Cost-based droop scheme with lower generation costs for microgrids', *IET Power Electron.*, 2014, **7**, (5), pp. 1171–1180

[7] Xia, Y., Peng, Y., Wei, W.: 'Tripple droop control method for AC microgrids', *IET Power Electron.*, 2017, **10**, (13), pp. 1705–1713

[8] Nasirian, V., Shafiee, Q., Guerrero, J.M., *et al.*: 'Droop-free distributed control for AC microgrids', *IEEE Trans. Power Electron.*, 2016, **31**, (2), pp. 1600–1617

[9] Pogaku, N., Prodanovic, M., Green, T.C.: 'Modeling, analysis and testing of autonomous operation of an inverter-based microgrid', *IEEE Trans. Power Electron.*, 2007, **22**, (2), pp. 613–625

[10] Katiraei, F., Irvani, M.R., Lehn, P.W.: 'Small-signal dynamic model of a microgrid including conventional and electronically interfaced distributed resources', *IET Gener. Transm. Distrib.*, 2007, **1**, (3), pp. 369–378

[11] Li, Z., Shahidepour, M.: 'Small-signal modeling and stability analysis of hybrid AC/DC microgrids', *IEEE Trans. Smart Grid*, 2019, **10**, (2), pp. 2080–2095

[12] Yan, Y., Shi, D., Bian, D., *et al.*: 'Small-signal stability analysis and performance evaluation of microgrids under distributed control', *IEEE Trans. Smart Grid*, 2019, **10**, (5), pp. 4848–4858

[13] Diaz, G., Gonzalez-Moran, C., Gomez-Aleixandre, J., *et al.*: 'Complex-valued state matrices for simple representation of large autonomous microgrids supplied by PQ and Vf generation', *IEEE Trans. Power Syst.*, 2009, **24**, (4), pp. 1720–1730

[14] Guo, X., Lu, Z., Wang, B., *et al.*: 'Dynamic phasors-based modeling and stability analysis of droop-controlled inverters for microgrid applications', *IEEE Trans. Smart Grid*, 2014, **5**, (6), pp. 2980–2987

[15] Iyer, S.V., Belur, M.N., Chandorkar, M.C.: 'A generalized computational method to determine stability of a multi-inverter microgrid', *IEEE Trans. Power Electron.*, 2010, **25**, (9), pp. 2420–2432

[16] Naderi, M., Khayat, Y., Shafiee, Q., *et al.*: 'Interconnected autonomous AC microgrids via back-to-back converters – part I: small-signal modeling', *IEEE Trans. Power Electron.*, 2020, **35**, (5), pp. 4728–4740

[17] Lou, G., Gu, W., Wang, J., *et al.*: 'Optimal design for distributed secondary voltage control in islanded microgrids: communication topology and controller', *IEEE Trans. Power Syst.*, 2019, **34**, (2), pp. 968–981

[18] Hassan, M.A., Abido, M.: 'Optimal design of microgrids in autonomous and grid-connected modes using particle swarm optimization', *IEEE Trans. Power Electron.*, 2011, **26**, (3), pp. 755–769

[19] Chung, I.Y., Liu, W., Cartes, D.A., *et al.*: 'Control methods of inverter-interfaced distributed generators in a microgrid system', *IEEE Trans. Ind. Appl.*, 2010, **46**, (3), pp. 1078–1088

[20] Yu, K., Ai, Q., Wang, S., *et al.*: 'Analysis and optimization of droop controller for microgrid system based on small-signal dynamic model', *IEEE Trans. Smart Grid*, 2016, **7**, (2), pp. 695–704

[21] He, J., Wu, X., Wu, X., *et al.*: 'Small-signal stability analysis and optimal parameters design of microgrid clusters', *IEEE Access*, 2019, **7**, pp. 36896–36909

[22] Askarzadeh, A.: 'A memory-based genetic algorithm for optimization of power generation in a microgrid', *IEEE Trans. Sustain. Energy*, 2018, **9**, (3), pp. 1081–1089

[23] Shariatzadeh, F., Kumar, N., Srivastava, A.: 'Optimal control algorithms for reconfiguration of shipboard microgrid distribution system using intelligent techniques', *IEEE Trans. Ind. Appl.*, 2017, **53**, (1), pp. 474–482

[24] Fisher, R.A.: 'The design of experiments' (Hafner, New York, 1971)

[25] Taguchi, G.: 'Quality engineering (Taguchi methods) for the development of electronic circuit technology', *IEEE Trans. Reliab.*, 1995, **44**, (2), pp. 225–229

[26] Coleman, D.E., Montgomery, D.C.: 'A systematic approach to planning for a designed industrial experiment', *Technometrics*, 1993, **35**, (1), pp. 1–12

[27] Marzband, M., Parhizi, N., Savaghebi, M., *et al.*: 'Distributed smart decision-making for a multi-microgrid system based on a hierarchical interactive architecture', *IEEE Trans. Energy Convers.*, 2016, **31**, (2), pp. 637–648

[28] Xiang, Y., Liu, J., Liu, Y.: 'Robust energy management of microgrid with uncertain renewable generation and load', *IEEE Trans. Smart Grid*, 2016, **7**, (2), pp. 1034–1043

[29] Rocabert, J., Luna, A., Blaabjerg, F., *et al.*: 'Control of power converters in AC microgrids', *IEEE Trans. Power Electron.*, 2012, **27**, (11), pp. 4734–4749

[30] Guerrero, J.M., García de Vicuña, L., Matas, J., *et al.*: 'Output impedance design of parallel-connected UPS inverters with wireless load-sharing control', *IEEE Trans. Ind. Electron.*, 2005, **52**, (4), pp. 1126–1135

[31] Vasquez, J.C., Guerrero, J.M., Luna, A., *et al.*: 'Adaptive droop control applied to voltage-source inverters operating in grid-connected and islanded modes', *IEEE Trans. Ind. Electron.*, 2009, **56**, (10), pp. 4088–4096

[32] He, J., Li, Y.W.: 'Analysis, design, and implementation of virtual impedance for power electronics interfaced distributed generation', *IEEE Trans. Ind. Appl.*, 2011, **47**, (6), pp. 2525–2538

[33] Guerrero, J.M., García de Vicuña, L., Matas, J., *et al.*: 'A wireless controller to enhance dynamic performance of parallel inverters in distributed generation systems', *IEEE Trans. Power Electron.*, 2004, **19**, (5), pp. 1205–1213

[34] Qoria, T., Gruson, F., Colas, F., *et al.*: 'Critical clearing time determination and enhancement of grid-forming converters embedding virtual impedance as current limitation algorithm', *IEEE J. Emerg. Sel. Top. Power Electron.*, 2020, **8**, pp. 1050–1061, in press

[35] Plackett, R.L., Burman, J.P.: 'The design of optimum multifactorial experiments', *Biometrika*, 1946, **33**, (4), pp. 305–325

[36] Costa, N.R., Zulema, J.L., Pereira, L.: 'Desirability function approach: a review and performance evaluation in adverse conditions', *Chemom. Intel. Lab. Syst.*, 2011, **107**, (2), pp. 234–244

[37] Altman, D.G.: 'Practical statistics for medical research' (Chapman and Hall/CRC, London, UK, 1990)